Universal Features of Electron Dynamics in Solar Cells with TiO 2 Contact: From Dye Solar Cells to Perovskite Solar Cells

ARTICLE *in* JOURNAL OF PHYSICAL CHEMISTRY LETTERS · SEPTEMBER 2015

Impact Factor: 7.46 · DOI: 10.1021/acs.jpclett.5b01696

THE JOURNAL OF PHYSICAL CHEMISTRY Letters

Letter

pubs.acs.org/JPCL

Universal Features of Electron Dynamics in Solar Cells with TiO_2 Contact: From Dye Solar Cells to Perovskite Solar Cells

Anna Todinova,[†] Jesús Idígoras,[†] Manuel Salado,[‡] Samrana Kazim,[‡] and Juan A. Anta*[,†]

[†]Área de Química Física, Universidad Pablo de Olavide, 41013 Sevilla, Spain

[‡]Abengoa Research, C/Energía Solar no. 1, Campus Palmas Altas, 41014 Sevilla, Spain

Supporting Information

ABSTRACT: The electron dynamics of solar cells with mesoporous TiO_2 contact is studied by electrochemical small-perturbation techniques. The study involved dye solar cells (DSC), solid-state perovskite solar cells (SSPSC), and devices where the perovskite acts as sensitizer in a liquid-junction device. Using a transport-recombination continuity equation we found that mid-frequency time constants are proper lifetimes that determine the current−voltage curve. This is not the case for the SSPSC, where a lifetime of ∼1 μs, 1 order of magnitude longer, is required to reproduce the current−voltage curve. This mismatch is attributed to the dielectric response on the mid-frequency component. Correcting for this effect, lifetimes lie on a common exponential trend with respect to open-circuit voltage. Electron transport times share a common trend line too. This universal behavior of lifetimes and transport times suggests that the main difference between the cells is the power to populate the mesoporous TiO_2 contact with electrons.

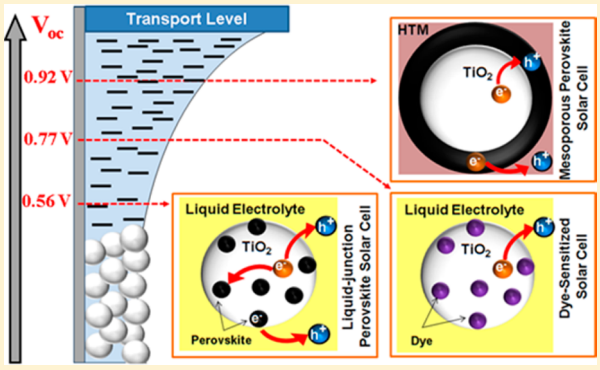

The discovery of the dye-sensitized solar cell (DSC)[1] in the early 90s initiated a new era of research for low-cost photovoltaics. The working principle of a DSC is based on the injection of electrons into nanostructured metal-oxide (TiO_2, ZnO) photoanodes from chemically adsorbed dye molecules, regenerated by a redox pair in a liquid electrolyte. The energy conversion efficiency potentially achievable with this concept, however, was hindered from the very beginning by stability issues. To overcome this drawback, much effort was devoted to replace the liquid electrolyte and the dye employed in the original device by more robust components, such as solid-state organic hole conductors and inorganic sensitizers, respectively.[2] In this context, the use of lead-organic halides (typically $CH_3NH_3PbI_3$) with perovskite crystal structure emerged in 2006.[3] These compounds were soon much appreciated as efficient sensitizers in DSC.

A major breakthrough took place in 2013 when Snaith's group demonstrated that the perovskite material in contact with an insulating mesoporous Al_2O_3 scaffold was capable of producing efficiencies exceeding 12%,[4] whereas a planar configuration yielded more than 15%.[5] Both results demonstrated that the perovskite material was not only a good light absorber but also an efficient charge "separator", in the sense that it is capable of conducting electrons and holes to external (selective) contacts with small recombination losses. This property was confirmed by Stranks et al.[6] and Xing et al.,[7] who estimated electron and hole diffusion lengths as long as 1 μm. The efficiencies demonstrated both in a planar[4,8] and in a mesoporous configuration[9] make perovskite solar cells (PSC) one of the most promising photovoltaic technologies to date.

Small perturbation techniques have been widely used to understand electron transport and recombination in solar cell devices like DSC and PSC.[10−12] In electrochemical impedance spectroscopy (EIS) a small sinusoidal modulation of the voltage is superimposed on a DC voltage and the resulting voltage/current impedance is analyzed. EIS makes it possible to obtain transport and recombination time constants along with internal resistances. Nevertheless, the parameters extracted from EIS will only have a physical meaning if the equivalent circuit used does truly resemble the real processes taking place in the device. Intensity-modulated photocurrent spectroscopy (IMPS) and intensity-modulated photovoltage spectroscopy (IMVS) a sinusoidal modulation of the light intensity (small enough to ensure a linear response) is applied and the frequency-dependent photocurrent or photovoltage response is obtained. Both IMPS and IMVS produce time constants that can be ascribed to transport and recombination processes occurring in the device,[11,12] in principle, without the need of an equivalent circuit.

In this work EIS, IMVS, and IMPS experiments have been carried out to compare the electron transport and recombination processes of devices that share the same photoanode: a mesoporous nanostructured TiO_2 film (Scheme 1). Hence, we used a DSC device as a reference system along with an intermediary system between DSC and a solid state perovskite cell (SSPSC). Inspired by the historical development that led

Received: August 5, 2015
Accepted: September 9, 2015

DOI: 10.1021/acs.jpclett.5b01696
J. Phys. Chem. Lett. 2015, 6, 3923−3930

Scheme 1. Solar Cells Analyzed in This Work[a]

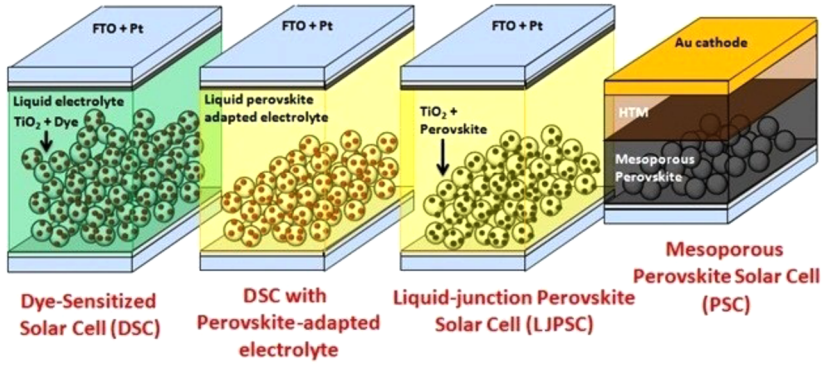

FTO/mp-TiO_2/**dye**/I_3^--I^-(acn/vn)/Pt/FTO ➡ FTO/mp-TiO_2/**dye**/ I_3^--I^-(ethylacetate)/Pt/FTO ➡
FTO/mp-TiO_2/**$CH_3NH_3PbI_3$**/ I_3^--I^-(ethylacetate)/Pt/FTO ➡ FTO/mp-TiO_2/**$CH_3NH_3PbI_3$**/ spiro-OmeTad/Au

[a]From left to right: high-performance DSC, DSC with an adapted liquid electrolyte and N719 dye as sensitizer, LJPCS with adapted liquid electrolyte and perovskite as sensitizer, and standard mesoporous SSPSC with Spiro-OMeTad as HTM. Red dots represent dye molecules and the black color stands for perovskite material.

to state-of-the-art PSC, we have chosen for this intermediary system a liquid-junction perovskite solar cell (LJPSC) where the perovskite is used as TiO_2 sensitizer in combination with a iodide-based liquid electrolyte, in the spirit of a quantum-dot sensitized solar cell. Although the main drawback of LJPSCs is the dissolution of the perovskite absorber by the liquid electrolyte, efficiencies of LJPSC between 3 and 6% were reported in previous works.[13,14] In spite of the limited operation time, the cells were stable enough to study electron transport and recombination in LJPSC by IMVS/IMPS.[15] Although DSC, LJPSC, and SSPSC were characterized by small perturbation techniques before,[11,12,15−17] no exhaustive study has been attempted on a complete series of devices following the historical development from DSC to SSPSC, to the best of our knowledge. This kind of study is very useful, as a lot can be learned from the comparison of different photovoltaic systems and technologies. It is possible to understand what make them different from a fundamental point of view, so the large amount of published data can be rationalized and clues to make further progress in the field can be provided.

Scheme 1 shows the different types of solar devices fabricated and studied by EIS, IMVS, and IMPS techniques in this work: (1) a high-performance DSC with C101 sensitizer and standard liquid electrolyte (acetonitrile/valeronitrile as solvent), (2) a DSC with N719 sensitizer and a perovskite-adapted electrolyte (ethyl acetate as solvent), (3) LJPSC with a perovskite as a sensitizer and a perovskite-adapted electrolyte, and (4) a "classical" mesoporous solid-state perovskite cell with Spiro-OMeTad as hole conducting material (HTM) (SSPSC). In order to get a unified picture, the results obtained from a solid-state DSC (SSDSC) reported in the literature have also been included in the comparison.[18]

Details of the experimental fabrication of the devices are in the Supporting Information. All devices share a mesoporous nanostructured TiO_2 film with a particle size of 20−30 nm, although the TiO_2 film thickness vary (from 9 μm of the high-performance DSC to less than one micron in SSPSC). The solar cells were characterized using stationary techniques ($J-V$ curves under simulated sunlight) and small perturbation techniques EIS/IMVS/IMPS. The small-perturbation analysis was carried out at open-circuit and under bias illumination from a LED of adjustable light intensity. Hence, the results at varying open-circuit potential reported in this paper are accomplished by varying the bias illumination. Details of the characterization procedures are also included in the Supporting Information.

Due to the limited operation time of the LJPSC devices, only one technique was used for the measurements. For each sample $J-V$ curves were recorded after the small perturbation experiment to verify that the performance of the cells had not been changed. To compare the results and reproducibility of the

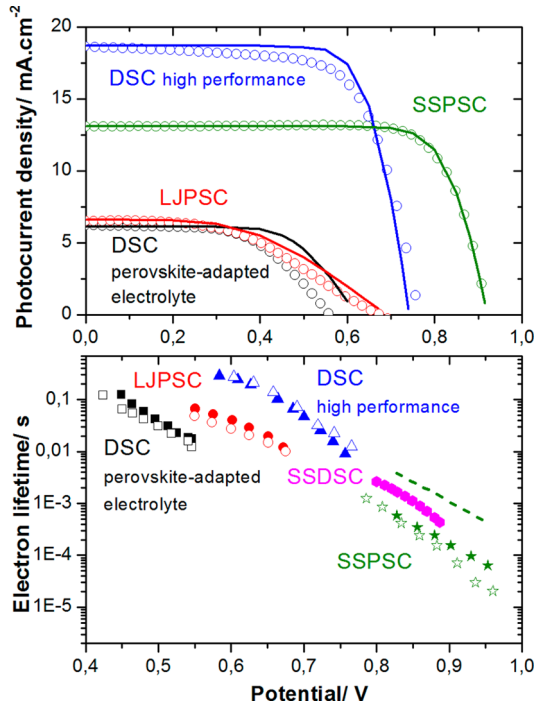

Figure 1. Top: $J-V$ curves of high-performance DSC, DSC with perovskite-adapted electrolyte, LJPSC, and SSPSC under 1 sun-AM 1.5G illumination. Lines stand for experimental data and symbols for the prediction of a continuity equation model (see text for details). Bottom: Comparison of characteristic times obtained from IMVS (empty symbols) and fitting of EIS spectra (filled symbols) for: high-performance DSC (fitted using transmission line model), DSC with perovskite-adapted electrolyte (nR-CPE model), LJPSC (nR-CPE model), SSPSC (nR-CPE model). Dashed line is corrected lifetimes for the SSPSC cell (see text for details).

DOI: 10.1021/acs.jpclett.5b01696
J. Phys. Chem. Lett. 2015, 6, 3923−3930

Table 1. Photovoltaic Parameters at 1 Sun and Small-Perturbation Data for Best Performing DSCs, LJPSC, SSPSC Cells[a]

cell	J_{sc}, mA/cm^2	V_{oc}, mV	fill factor, %	efficiency, %	β	α	$\tau_{V_{oc}(1sun)}$, s^{-1}
DSC (high performance)	18.9	766	66	9.6	0.74	0.22	$\sim 10^{-2}$
DSC (per. adapted electrolyte)	6.2	559	57	2.0	0.56/0.59	0.16/0.31	$\sim 10^{-2}$
LJPSC	7.1	680	48	2.3	0.43	0.12	$\sim 10^{-2}$
SSPSC	13.1	921	77	9.3	0.57/0.66	flat	$10^{-4}/5 \times 10^{-5}$

[a] β is the recombination parameter, α is the trap parameter, and $\tau_{V_{oc}(1sun)}$ the mid-frequency time constant at the experimental open circuit photovoltage at 1 sun obtained from EIS data.

different LJPSC cells employed in this work, $J-V$ curves and open-circuit voltage decay (OCVD) data were used as a control (see Figure S1 in Supporting Information).

Figure 1 (top), shows the $J-V$ curves of high-performance DSC, DSC with perovskite adapted electrolyte, LJPSC, and SSPSC. The photovoltaic parameters of these cells are shown on Table 1. In the case of DSC with perovskite-adapted electrolyte, the lower performance with respect to the high-performance DSC[19] is due to the use of another dye (N719), a smaller thickness of TiO_2 layer and the absence of scattering layer. Furthermore, the nonoptimized electrolyte produces faster recombination so that the fill factor and the 1 sun open-circuit photovoltage decrease.

When the $CH_3NH_3PbI_3$ sensitizer was used instead of the dye, the efficiency of the best performing LJPSC cell was 2.3%. Thanks to the higher photocurrent and photovoltage, LJPSC show higher efficiency than DSC with perovskite-adapted liquid electrolyte in spite of a lower fill factor. The SSPSC device showed an efficiency of 9.3%, mainly due to a large open-circuit photovoltage, characteristicof perovskites with spiro-OMeTad as HTM.

For all cells, the impedance spectra were measured under illumination at open circuit. Figure 2 shows EIS spectra and corresponding Bode plots for DSCs, LJPSC, and SSPSC.

Fittings to the equivalent circuits used in this work are included in the graphs. Electrolyte-based solar cells spectra have two arcs, whereas SSPSC shows three, corresponding to the same number of time constants, featured as peaks or shoulders in the Bode plot. The size and position of the arcs and the time constant varied monotonically with the applied bias (illumination light intensity). All three arcs of SSPSC could be clearly seen at lower potentials (see Supporting Information Figure S2).

The most common equivalent circuit, which allowed to interpret impedance spectra for DSC for over a decade is based on a transmission line model proposed by Bisquert and co-workers (see Supporting Information Figure S3).[20] The model is based on a distributed element containing a diffusion-recombination transmission line. This gives rise to a mid-frequency arc containing a 45°-slope straight line at high frequency, accounting for electron diffusion in the TiO_2 layer, and a RC element (R − resistor, C − capacitor) where resistance and capacitance are

$$R_{rec} = R_0 \exp\left(-\beta \frac{qV}{k_B T}\right) \quad (1)$$

$$C_\mu = C_0 \exp\left(\alpha \frac{qV}{k_B T}\right) \quad (2)$$

where, R_0 and C_0 are constants, q is the elementary charge, k_B is Boltzmann's constant, T is the absolute temperature, β and α are dimensionless parameters, and V is the voltage (electrical potential). It is well known that for a DSC, the recombination resistance is attributed to the processes occurring in the TiO_2/electrolyte interface, whereas C_μ is a "chemical capacitance" that accounts for accumulation of electrons in localized states located in the TiO_2 band gap.

The parameter β can be related to the order of the recombination reaction with respect to free electrons, which is the inverse of the diode ideality factor.[21,22] For a TiO_2 mesoporous electrode in DSC the values of β are usually higher than 0.5.[19] The trap parameter α is a dimensionless quantity related to the mean energy of the exponential distribution of localized states in the TiO_2.[23] This parameter controls the voltage dependence of the accumulation of electrons in the localized states of the TiO_2 bandgap and hence the slope of the capacitance versus potential in a semilogarithmic plot.

In Figure 3, the electron recombination resistance and chemical capacitance for the two DSC configurations studied here are shown. The recombination resistance has a clear exponential behavior with $\beta > 0.5$ (see Table 1) in both cases. As expected, R_{rec} is larger for the cells with the larger V_{OC}. The capacitance also has exponential behavior with $\alpha = 0.2-0.3$, in accordance with the typical values obtained for DSC.[19] For the two DSC, and correcting the capacitance for the film thickness by linear scaling, a small band shift due to the different electrolyte composition could be observed. However, the capacitance of the high-performance DSC reaches larger values due to the larger 1 sun V_{OC}, in agreement with eq 2.

Interpretation of impedance spectra of SSPSC is not straightforward.[17,24] The most frequently used and simple model is the one based on several RC elements in series, where the number of RC elements depends on the amount of semicircles appearing in the EIS spectrum (time features in the Bode plot).[16,25,26] In addition, the capacitance C could be substituted by the constant phase element (nR-CPE model).[16] The data obtained for CPE element could be recalculated into the ones corresponding to capacitance. The nR-CPE equivalent cirquit is shown in Supporting Information Figure S2.

For a universal description of the experimental data, we have used the nR-CPE equivalent circuit for all devices except the high-performance DSC. In Figure 2 the quality of the fittings of both equivalent circuits can be assessed. At this point it is important to stress the equivalence observed between the recombination arc in the transmission line model (defined by eqs 1, 2 and 5) and the mid-frequency arc in the nR-CPE model. In Supporting Information Figure S4, Nyquist and Bode plots for EIS and IMVS are compared. In IMVS the time constant is obtained from the frequency-modulated photovoltage response. IMVS spectra usually consist of one arc with a time constant defined by

$$\tau_n^{IMVS} = \frac{1}{\omega_{min}} \quad (3)$$

DOI: 10.1021/acs.jpclett.5b01696
J. Phys. Chem. Lett. 2015, 6, 3923−3930

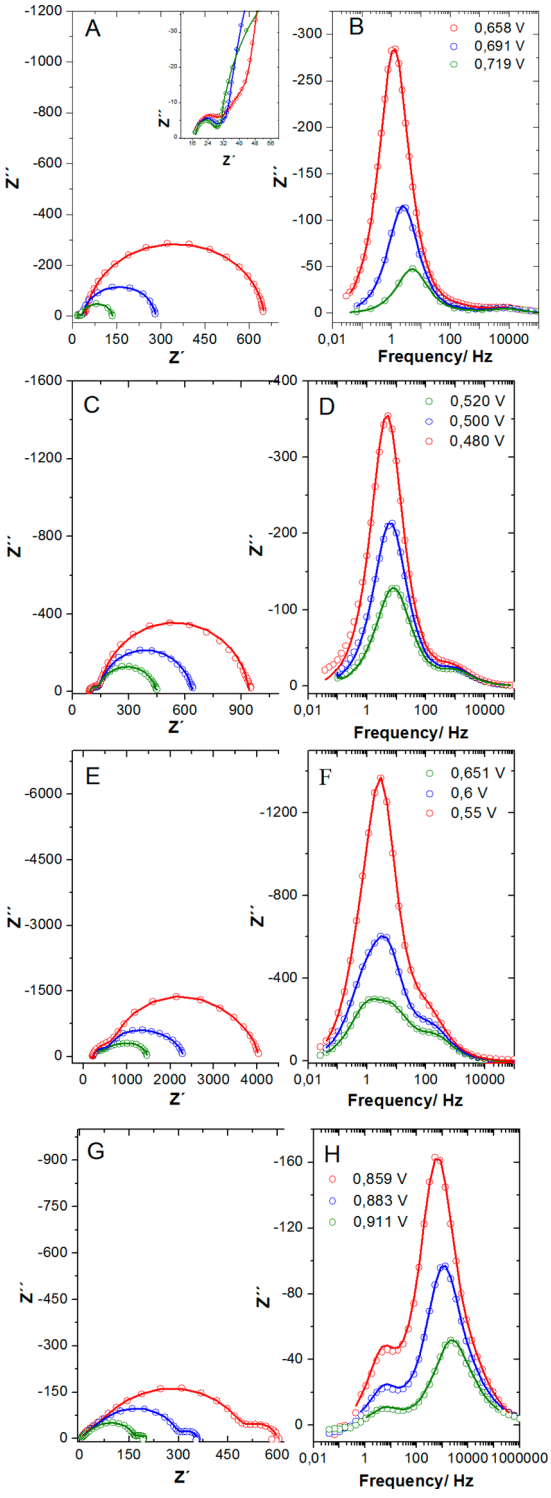

Figure 2. EIS Nyquist spectra for (A) high-performance DSC. Inset shows high frequency region. (C) DSC with perovskite-adapted electrolyte. (E) LJPSC, (G) SSPSC, and Bode plots for (B) high-performance DSC, (D) DSC with perovskite-adapted electrolyte, (F) LJPSC, and (H) SSPSC. The points stand for experimental data, the lines are the fitting with transmission line model (high-performance DSC), nR-CPE model for DSC with perovskite-adapted electrolyte, LJPSC, SSPSC, where *n* is the number of R-CPE elements (2 or 3).

As observed in previous works from the authors,[16] the IMVS time constant coincides with the RC time constant of the EIS

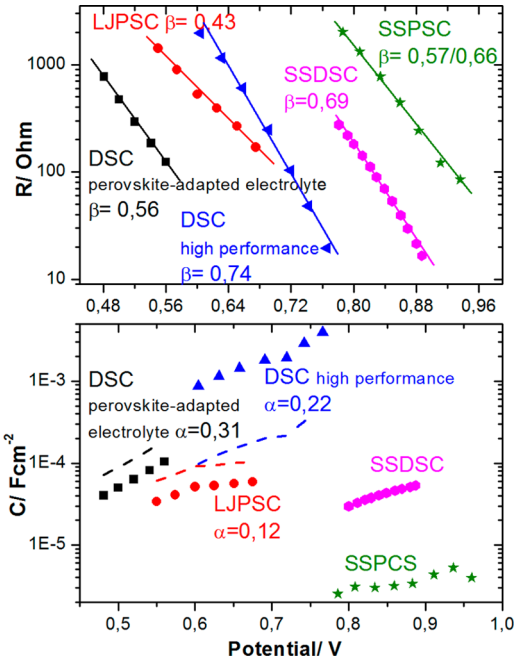

Figure 3. Comparison of mid-frequency resistance (top) and mid-frequency capacitance (bottom) for high-performance DSC, DSC with perovskite-adapted electrolyte, LJPSC, and SSPSC cells. For the sake of comparison, published data for SSDSC[18] are included in the graph. Dashed lines are capacitances corrected for TiO_2 film thickness.

mid-frequency arc

$$\tau_{\mathrm{mid}}^{\mathrm{EIS}} = R_{\mathrm{mid}} \cdot C_{\mathrm{mid}} \tag{4}$$

In Supporting Information Figures S5, S6, S7, and S8, the mid-frequency time constants obtained by the different procedures are compared. This confirms that the mid-frequency time constant (obtained by following the maxima of the peaks on Bode plots) of the corresponding EIS spectra coincides with IMVS time constant in all cases, although the slope is slightly different for SSPSC. In the classical transmission line model of DSC, an electron recombination lifetime can be obtained from

$$\tau_{\mathrm{rec}}^{\mathrm{EIS}} = R_{\mathrm{rec}} \cdot C_{\mu} \tag{5}$$

where R_{rec} and C_{μ} are defined by eqs 1 and 2. This lifetime coincides with the mid-frequency EIS time constant and with the IMVS time constant in the case of the high-performance DSC. For the rest of the electrolyte-based cells, the agreement is only partial, showing the limited validity of this model, in particular for cells where the perovskite is involved. Electron lifetimes extracted from OCVD are also close to the mid-frequency lifetimes in all electrolyte-based cells. All these results suggest that the mid-frequency time constant is a recombination lifetime, and that the resistance of the mid-frequency RC circuit element is a recombination resistance accounting for charge transfer across a particular interface in the solar cell.

The R_{mid} and C_{mid} extracted from the fit to the nR-CPE model, together with those extracted from the transmission line model for DSC (called R_{rec} and C_{μ}), are shown in Figure 3. For the sake of comparison, data from solid-state DSC(SSDSC) with Spiro-OMeTad as HTM[18] have been included. We observe exponential resistance in all devices. As this is the prediction of eq 1, this feature also points to the recombination character of this magnitude. However, the β-parameter changes for the

DOI: 10.1021/acs.jpclett.5b01696
J. Phys. Chem. Lett. 2015, 6, 3923−3930

different types of cells, which is a signature of different recombination mechanisms. As mentioned earlier, β is well larger than 0.5 for DSC, in particular for the high-performance cell. In contrast, the introduction of the perovskite as sensitizer takes this parameter below 0.5. For the SSPSC, β is again larger than 0.5, although it is still smaller than for a standard DSC. A β-parameter larger than 0.5 is an evidence of charge transfer from localized states in the semiconductor to electron acceptors in the liquid electrolyte.[27,28] A β-parameter smaller than 0.5 could be due to charge transfer across a solid heterojunction.[29,30] In the case of LJPSC, the perovskite covering of the TiO_2 could be dense enough to form a heterojunction. TiO_2 thickness in LJPSC is much larger than the one usually used in SSPSC configurations; therefore, the pore filling in LJPSC might not be complete. As a consequence, although TiO_2/electrolyte interface still plays an important role in the recombination process, a new interface with the perovskite could be involved, which decreases β. For the SSPSC, the data collected here does not allow us to establish unambiguously what is the main recombination pathway. However, the smaller values of β systematically obtained for these cells suggest that TiO_2/PS and PS/HTM interfaces are involved in the recombination loss. However, there are other factors that can affect the slope of the resistance, as discussed below. Regardless of the nature of recombination, it can be observed, as a general rule, that the recombination resistance at the same voltage is always larger for cells with larger 1 sun V_{OC}.

Results for the mid-frequency capacitance C_{mid} show that this quantity behaves exponentially in accordance to eq 2 except for SSPSC. Therefore, we can infer that for electrolyte-based solar cells and SSDSC $C_{mid} = C_\mu$. In striking contrast, SSPSC mid-frequency capacitance remains basically independent from the voltage.

We propose the following interpretation of the small-perturbation results. Bisquert and co-workers[24] proposed recently a simplified equialent circuit for perovskite solar cells in which two time constants are likely to appear

$$\tau_1 = (R_{rec} + R_{dr})C_{dr} \tag{6}$$

$$\tau_2 = \frac{R_{rec}R_{dr}}{R_{rec} + R_{dr}}C_\mu \tag{7}$$

where R_{dr} and C_{dr} account for the dielectric response of the perovskite layer. The dielectric capacitance is given by

$$C_{dr} = \frac{A\varepsilon_r\varepsilon_0}{d} \tag{8}$$

with ε_r being the relative dielectric constant. This is a frequency dependent quantity whose high frequency limit determines the geometric capacitance of the device. Importantly, this is a constant value, voltage independent. For $A = 0.5$ cm^2, $d = 500$ nm, $\varepsilon_r = 24$,[31] C_{dr} (geometric) $\sim 2 \times 10^{-8}$ F.

The results obtained from our small-perturbation analysis of SSPSC suggest that the mid-frequency time constant obeys eq 6 with $R_{rec} \gg R_{dr}$ and that there is an important geometric character in the capacitance, which makes it bias independent. However, the experimental capacitance values lie between 2.5 and 6×10^{-6} F, which is 2 orders of magnitude larger than the theoretical value mentioned above. This discrepancy seems to be related to the roughness of the TiO_2 mesoporous electrode. For a thickness of ~0.5−1 μm, this is around 100, which would account for the observed difference. It must also be taken into account that a huge variation of the dielectric constant with frequency and illumination has been reported.[31,32]

According to this interpretation, the resistance extracted from the mid-frequency feature of the SSPSC EIS spectrum and from the IMVS experiment still retains a recombination character that explains the behavior observed in Figure 3, top. However, the contribution of the dielectric resistance in eq 6 can modify the potential dependence. As the dielectric resistance can vary substantially with the quality of the perovskite film, the thickness of the active layer, among other parameters, the β-parameter can have very distinct values for devices prepared under different conditions.[16,30]

The comparison of the mid-frequency characteristic times for various devices obtained by IMVS and EIS are shown in Figure 1. The EIS results are obtained, as discussed before, using the transmission line model for the high-performance DSC and the nR-CPE equivalent circuit for the rest of the devices. For sensitized, electrolyte-based solar cells, the characteristic times are longer for the device showing the larger 1 sun V_{OC}, as expected from true recombination lifetimes. The most interesting feature of the whole picture is that the mid-frequency times for all studied devices lie on a single trend line that varies exponentially with open-circuit photovoltage. Although the time constants obtained for SSPSC are not pure recombination lifetimes (as indicated by eq 6 and explained below), this observation indicates that the main difference between solar cells is the position of Fermi level or accumulated electron density in the mesoporous TiO_2 contact. The higher up is the Fermi level (the larger the density), the faster is the charge transfer to electron acceptors and hence the recombination loss.[22,27,28,33] This interpretation is corroborated when looking at IMPS data, as discussed below.

IMPS has been used to obtain information on charge transport. So far, there was no report on the comparison of characteristic transport times for DSC, LJPSC, and SSPSC. The characteristic IMPS times or IMPS time constants, corresponding to the maxima in the Bode plots (shown in Supporting Information Figure S9), are shown in Figure 4. Two time

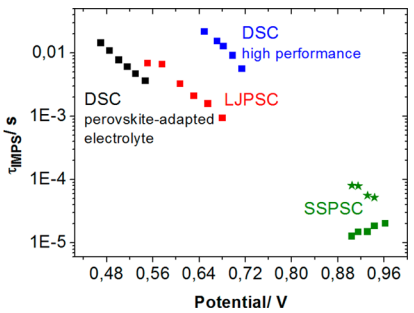

Figure 4. IMPS times for high-performance DSC, DSC with perovskite-adapted electrolyte, LJPSC, and SSPSC.

constants are observed in the IMPS spectrum. However, for the SSPSC, the evolution of the time constant with the bias in the ~10^{-5} s range follows a reverse trend to the rest.

We attribute the longer time constant to electron transport in TiO_2. Similar results were found in previous studies for the same type of cells (electron diffusion coefficient of around 10^{-6}−10^{-7} cm^2/s for electrolyte-based cells).[12] Furthermore, in complete analogy to the lifetimes of Figure 1, the TiO_2 transport times appear to be on a single universal trend line with respect to potential. This is again a consequence of the position of the

DOI: 10.1021/acs.jpclett.5b01696
J. Phys. Chem. Lett. 2015, 6, 3923−3930

Fermi level in the TiO_2 contact for the different types of solar cells. In a device with a larger V_{OC} at 1 sun, as is the case with the SSPSC, the Fermi level is higher up in the energy scale. According to the multiple-trapping model,[34−36] electrons are closer on average to the transport level, and hence, they move faster, yielding a shorter characteristic time in the IMPS experiment. This is described by the equation

$$D_n = D_0 e^{(1-\alpha)(E_f(n)-E_f^0)/k_BT} \tag{9}$$

where $E_f(n)$ and E_f^0 are the density dependent Fermi level and Fermi level in the dark, respectively, and D_0 is the dark diffusion coefficient. Equation 9 predicts an exponential dependence of the diffusion coefficient (and hence the time constant) with respect to bias potential, as observed in the experiments. In addition to this, band shifts also take place, detected in the capacitance data of Figure 3. This produces parallel lines in the transport times as observed in Figure 4.

A smaller time constant was also found for SSPSC in a recent work.[16] This time constant shows a reverse trend with voltage, a feature that does not exist for cells containing liquid electrolyte. However, the process corresponding to hole transport in SSDSC with Spiro-OMeTad as HTM, was observed before.[18] Therefore, this faster time constant could be assigned to hole transport in the HTM material. On the other hand, the detection of transport *inside* the perovskite film is ruled out, as this is too fast to be caught by the frequency range of the experiment. The reported electron diffusion coefficient of $CH_3NH_3PbCl_3$ is around 0.02 cm^2/s,[6] which for a film thickness of, for instance, 200 nm, would produce a transport signal at frequencies close to 50 MHz, well above the upper frequency limit of the IMPS experiment.

To provide a more complete picture of the results obtained, the $J-V$ curves shown in Figure 1 were reconstructed from the small perturbation data. To do so, a continuity equation model for charge carriers in the active layer was used. The following equation was numerically solved[16]

$$\frac{\partial n(x,t)}{\partial t} = \frac{\partial}{\partial n}\left[D_n(n)\frac{\partial n}{\partial x}\right] + G(x) - k_0 n^\delta \tag{10}$$

where $n(x,t)$ is the total density of electron−hole pairs generated in the active layer. For a DSC-type solar cell, this is the photogenerated electrons accumulated in the mesoporous TiO_2 (compensated by holes in the electrolyte).[37] An analogous picture holds for the perovskite-based cells, as electrons injected into the TiO_2 are compensated by holes generated in the perovskite or in the HTM layer. The right-hand side of eq 10 contains a *transport* term, governed by D_n, a density-dependent (thus voltage-dependent) diffusion coefficient given by eq 9, a *generation* term $G(x)$, which depends on the absorption spectrum of the organic dye or the perovskite, and a *recombination* contribution, where k_0 is a constant and δ the reaction order for recombination of electrons and holes. It has to be noted that, based on the information gathered by the IMPS experiment, only transport of electrons in the TiO_2 film is considered in eq 10, as this is the *slowest* process taking place in the cell. The spatial derivative $J = \delta n(x)/\delta x$ at $x = 0$ (external collection contact of electrons) yields the photocurrent for given values of the potential V. Details of the numerical solution of this equation can be found in the Supporting Information.

The key point in eq 10 is the recombination term, which defines the small perturbation recombination constant (inverse of the small-perturbation lifetime). For a typical DSC, this is defined by[22]

$$\begin{aligned} k_{rec}(n(V)) &= (\tau_{rec})^{-1} \\ &= k_0 \exp\{((\beta-\alpha)V)/(k_BT)\} \\ &= k^0\left(\frac{n}{n^0}\right)^{\frac{\beta-\alpha}{\alpha}} \end{aligned} \tag{11}$$

Hence, the reaction order is $\delta = (\beta - \alpha)/\alpha$. Assuming that the limiting transport is that of electrons in TiO_2, eqs 9, 10, and 11 make it possible to generate the $J-V$ curve of the device from the small perturbation lifetime (measured at 1 sun V_{OC}), and the values of α and β. Additionally, the effect of the series resistance, also obtainable from the EIS measurements, can be taken into account in the calculation. Results are shown in Figure 1, where they are compared with the experimental $J-V$ curves.

The main objective of the modeling is to ascertain whether the small-perturbation mid-frequency time constant justifies the V_{OC} measured at 1 sun and can reproduce the $J-V$ curve. In other words, is this quantity a real recombination lifetime? At this point, it is important to note that the generation term contains a prefactor (accounting for dye loading, injection yields, etc.), which is adjusted to reproduce the experimental J_{SC}. The rest of the parameters of the model are taken or estimated from the small-perturbation measurements. Hence, for all cells except the SSPSC, the β parameters are taken from the data in Table 1, with a constant value of $\alpha = 0.3$. k_0 was adjusted to match the small perturbation lifetime at 1 sun V_{OC} (last column in Table 1) according to eq 11. This procedure gave a fair reproduction of the experimental $J-V$ curve with a maximum error of 60 mV in the estimation of the 1 sun V_{OC}. This result demonstrates that the time constants extracted from the IMVS and the mid-frequency arc in EIS are true recombination lifetimes, that is, the ones that govern the $J-V$ curve and the overall performance of the cell.

However, the same procedure failed for the SSPSC because it was not possible to fit the $J-V$ curve with a lifetime at 1 sun of $\sim 10^{-4}$ s and a EIS β-parameter of ~0.5−0.6. An additional complication was that the mid-frequency capacitance is flat, meaning that it is not chemical and the trap parameter α was then undefined (or at least, it could not be measured). This does not mean, however, that the general continuity model of eq 10 does not hold in this case. In fact, it provides an opportunity to test the accuracy of the small-perturbation analysis and the real value of the lifetime for the solid-state perovskite cell. In this regard, O'Regan and co-workers reported recently kinetic data for perovskite cells with flat configuration.[38] These authors reported two time constants in transient photovoltage experiments, finding that only one of them, of the range of ~1 μs was the one consistent with the measured dark currents. They also reported estimated reaction orders ranging between 2.4 and 4.4. Following these indications, we tried to fit the experimental $J-V$ curve with τ_{rec} (V = 0.92 V) ~ 1 μs and α = 0.2, β = 0.7, corresponding to a reaction order of δ = 2.5. These parameters, together with the series resistance extracted from EIS, showed excellent agreement with the experimental $J-V$ curve. This outcome confirms that the real recombination lifetime is in the range of microseconds at open-circuit and 1 sun for a typical SSPSC device. However, this is more than 1 order of magnitude than the one found in the small perturbation analysis. The origin of this discrepancy was suggested in the discussion above: the mid-frequency time constant of eq 6 is not a real recombination lifetime because the dielectric resistance and the geometric

DOI: 10.1021/acs.jpclett.5b01696
J. Phys. Chem. Lett. 2015, 6, 3923−3930

capacitance also affect the time resonance observed in the IMVS and EIS experiments. However, it is a good approximation and the resistance can still be considered as a recombination resistance. In fact, a lifetime of 10^{-6} s at 1 sun V_{OC} would place the SSPSC data in line with the high-performance DSC lifetimes (dashed line in Figure 1 bottom).

Very recently,[39] hysteresis in perovskite solar cells has been explained in terms of ion migration inside the perovskite film. This migration modifies the internal electrical field acting on the electrons and holes that produce the measured photocurrent. If the scan rate is too fast, a significant hysteresis can be observed. In the modeling, we have assumed that the preconditioning and the scan rate is such that the cell is at a pseudostationary condition,[40] and the ions have had enough time to relax to their final positions. Hence, the potential V in eq 11 is the internal potential arising from this situation and the potential for which the equation is solved and the current obtained. In any case, as hysteresis only affects significantly the fill factor and no so much the V_{OC}, our conclusions regarding the lifetime and the V_{OC} extracted from the modeling would not be affected.

In conclusion, we have performed a global analysis of three types of cells that share the same mesoporous TiO_2 contact. $J-V$ curves and small-perturbation (IMVS/IMPS/EIS) measurements have been carried out. A correspondence between the IMVS time constant and the time constant of the mid-frequency EIS arc has been found, which is attributed to recombination loss in the device. For electrolyte-based solar cells only, this is found to be consistent with the recombination lifetime that governs the stationary $J-V$ curve and the 1 sun V_{OC}, as predicted by a continuity equation model that takes into account generation, transport and recombination of charge carriers. In contrast, the mid-frequency time constant of the solid-state perovskite solar cell is affected by a dielectric contribution, which means that it is not a real recombination lifetime. This is confirmed by the fact that the continuity equation model fails to reproduce the $J-V$ curve with this time constant. However, the recombination resistance followed an exponential behavior for all the devices. The introduction of the perovskite sensitizer reduces the β-parameter, which may indicate the participation of the solid heterojunction in the recombination mechanism. Unlike the capacitance of DSC devices and LJPSC, which are chemical due to their exponential behavior, it is flat in the case of SSPSC. This can be attributed to a geometrical nature of the capacitance in the solid perovskite device. For all the devices, IMPS data show transport times corresponding to electron transport in the TiO_2. However, in devices with solid HTM, a second time constant with a reverse bias dependence is observed. This transport time is faster and is attributed to the motion of holes in HTM material. In general, electron lifetimes and TiO_2 transport times fall on a single trend line with respect to open circuit potential. This shows that the main difference between the three types of solar cells is the ability of the absorber (either the dye or the perovskite) to generate carriers and to inject electrons into the TiO_2.

■ ASSOCIATED CONTENT

Supporting Information

The Supporting Information is available free of charge on the ACS Publications website at DOI: 10.1021/acs.jpclett.5b01696.

Details of the preparation and characterization of the devices. Details on the $J-V$ curve numerical model. Figures S1 and S2, including comparison of lifetimes from different procedures and techniques, and for different devices. Bode plots of EIS, IMVS, and IMPS. (PDF)

■ AUTHOR INFORMATION

Corresponding Author

*E-mail: anta@upo.es.

Notes

The authors declare no competing financial interest.

■ ACKNOWLEDGMENTS

We thank Junta de Andalucía for financial support via grant FQM 1851. We thank Ministerio de Economía y Competitividad of Spain under grant MAT2013-47192-C3-3-R.

■ REFERENCES

(1) O'Regan, B.; Gratzel, M. A Low-Cost, High-Efficiency Solar-Cell Based on Dye-Sensitized Colloidal Tio2 Films. *Nature* **1991**, *353*, 737−740.

(2) Snaith, H. J. Perovskites: The Emergence of a New Era for Low-Cost, High-Efficiency Solar Cells. *J. Phys. Chem. Lett.* **2013**, *4*, 3623−3630.

(3) Kojima, A.; Teshima, K.; Shirai, Y.; Miyasaka, T. Novel Photoelectrochemical Cell with Mesoscopic Electrodes Sensitized by Lead-Halide Compounds (5). *ECS Meet. Abstr., 212th* **2007**, *MA2007−02*, 352−352.

(4) Ball, J. M.; Lee, M. M.; Hey, A.; Snaith, H. Low-Temperature Processed Mesosuperstructured to Thin-Film Perovskite Solar Cells. *Energy Environ. Sci.* **2013**, *6*, 1739−1743.

(5) Liu, M.; Johnston, M. B.; Snaith, H. J. Efficient Planar Heterojunction Perovskite Solar Cells by Vapour Deposition. *Nature* **2013**, *501*, 395−398.

(6) Stranks, S. D.; Eperon, G. E.; Grancini, G.; Menelaou, C.; Alcocer, M. J. P.; Leijtens, T.; Herz, L. M.; Petrozza, A.; Snaith, H. J. Electron-Hole Diffusion Lengths Exceeding 1 Micrometer in an Organometal Trihalide Perovskite Absorber. *Science* **2013**, *342*, 341−344.

(7) Xing, G.; Mathews, N.; Sun, S.; Lim, S. S.; Lam, Y. M.; Grätzel, M.; Mhaisalkar, S.; Sum, T. C. Long-Range Balanced Electron- and Hole-Transport Lengths in Organic-Inorganic $CH_3NH_3PbI_3$. *Science* **2013**, *342*, 344−347.

(8) Zhou, H.; Chen, Q.; Li, G.; Luo, S.; Song, T.; Duan, H.-S.; Hong, Z.; You, J.; Liu, Y.; Yang, Y. Interface Engineering of Highly Efficient Perovskite Solar Cells. *Science* **2014**, *345*, 542−546.

(9) Burschka, J.; Pellet, N.; Moon, S.-J.; Humphry-Baker, R.; Gao, P.; Nazeeruddin, M. K.; Grätzel, M. Sequential Deposition as a Route to High-Performance Perovskite-Sensitized Solar Cells. *Nature* **2013**, *499*, 316−319.

(10) Dloczik, L.; Ileperuma, O.; Lauermann, I.; Peter, L. M.; Ponomarev, E. A.; Redmond, G.; Shaw, N. J.; Uhlendorf, I. Dynamic Response of Dye-Sensitized Nanocrystalline Solar Cells: Characterization by Intensity-Modulated Photocurrent Spectroscopy. *J. Phys. Chem. B* **1997**, *101*, 10281−10289.

(11) Fabregat-Santiago, F.; Garcia-Belmonte, G.; Mora-Sero, I.; Bisquert, J. Characterization of Nanostructured Hybrid and Organic Solar Cells by Impedance Spectroscopy. *Phys. Chem. Chem. Phys.* **2011**, *13*, 9083−9118.

(12) Pockett, A.; Eperon, G. E.; Peltola, T.; Snaith, H. J.; Walker, A.; Peter, L. M.; Cameron, P. J. Characterization of Planar Lead Halide Perovskite Solar Cells by Impedance Spectroscopy, Open-Circuit Photovoltage Decay, and Intensity-Modulated Photovoltage/Photocurrent Spectroscopy. *J. Phys. Chem. C* **2015**, *119*, 3456−3465.

(13) Kojima, A.; Teshima, K.; Shirai, Y.; Miyasaka, T. Organometal Halide Perovskites as Visible-Light Sensitizers for Photovoltaic Cells. *J. Am. Chem. Soc.* **2009**, *131*, 6050−6051.

(14) Im, J.-H.; Lee, C.-R.; Lee, J.-W.; Park, S.-W.; Park, N.-G. 6.5% Efficient Perovskite Quantum-Dot-Sensitized Solar Cell. *Nanoscale* **2011**, *3*, 4088−4093.

DOI: 10.1021/acs.jpclett.5b01696
J. Phys. Chem. Lett. 2015, 6, 3923−3930

(15) Zhao, Y.; Zhu, K. Charge Transport and Recombination in Perovskite (CH_3NH_3)PbI_3 Sensitized TiO_2 Solar Cells. *J. Phys. Chem. Lett.* **2013**, *4*, 2880−2884.
(16) Guillén, E.; Ramos, F. J.; Anta, J. A.; Ahmad, S. Elucidating Transport-Recombination Mechanisms in Perovskite Solar Cells by Small-Perturbation Techniques. *J. Phys. Chem. C* **2014**, *118*, 22913−22922.
(17) Dualeh, A.; Moehl, T.; Tétreault, N.; Teuscher, J.; Gao, P.; Nazeeruddin, M. K.; Grätzel, M. Impedance Spectroscopic Analysis of Lead Iodide Perovskite-Sensitized Solid-State Solar Cells. *ACS Nano* **2014**, *8*, 362−373.
(18) Li, F.; Jennings, J. R.; Wang, Q.; Chua, J.; Mathews, N.; Mhaisalkar, S. G.; Moon, S.-J.; Zakeeruddin, S. M.; Grätzel, M. Determining the Conductivities of the Two Charge Transport Phases in Solid-State Dye-Sensitized Solar Cells by Impedance Spectroscopy. *J. Phys. Chem. C* **2013**, *117*, 10980−10989.
(19) Idígoras, J.; Pellejà, L.; Palomares, E.; Anta, J. A. The Redox Pair Chemical Environment Influence on the Recombination Loss in Dye-Sensitized Solar Cells. *J. Phys. Chem. C* **2014**, *118*, 3878−3889.
(20) Bisquert, J. Theory of the Impedance of Charge Transfer via Surface States in Dye-Sensitized Solar Cells. *J. Electroanal. Chem.* **2010**, *646*, 43−51.
(21) Bisquert, J.; Mora-Seró, I. Simulation of Steady-State Characteristics of Dye-Sensitized Solar Cells and the Interpretation of the Diffusion Length. *J. Phys. Chem. Lett.* **2010**, *1*, 450−456.
(22) Anta, J. A.; Idígoras, J.; Guillén, E.; Villanueva-Cab, J.; Mandujano-Ramírez, H. J.; Oskam, G.; Pellejà, L.; Palomares, E. A Continuity Equation for the Simulation of the Current−Voltage Curve and the Time-Dependent Properties of Dye-Sensitized Solar Cells. *Phys. Chem. Chem. Phys.* **2012**, *14*, 10285−10299.
(23) Bisquert, J. Chemical Capacitance of Nanostructured Semiconductors: Its Origin and Significance for Nanocomposite Solar Cells. *Phys. Chem. Chem. Phys.* **2003**, *5*, 5360−5364.
(24) Bisquert, J.; Bertoluzzi, L.; Mora-Sero, I.; Garcia-Belmonte, G. Theory of Impedance and Capacitance Spectroscopy of Solar Cells with Dielectric Relaxation, Drift-Diffusion Transport, and Recombination. *J. Phys. Chem. C* **2014**, *118*, 18983−18991.
(25) Zhang, J.; Pauporté, T. Effects of Oxide Contact Layer on the Preparation and Properties of $CH_3NH_3PbI_3$ for Perovskite Solar Cell Application. *J. Phys. Chem. C* **2015**, *119*, 14919−14928.
(26) Xu, X.; Liu, Z.; Zuo, Z.; Zhang, M.; Zhao, Z.; Shen, Y.; Zhou, H.; Chen, Q.; Yang, Y.; Wang, M. Hole Selective NiO Contact for Efficient Perovskite Solar Cells with Carbon Electrode. *Nano Lett.* **2015**, *15*, 2402−2408.
(27) Gonzalez-Vazquez, J. P.; Oskam, G.; Anta, J. A. Origin of Nonlinear Recombination in Dye-Sensitized Solar Cells: Interplay between Charge Transport and Charge Transfer. *J. Phys. Chem. C* **2012**, *116*, 22687−22697.
(28) Bisquert, J.; Fabregat-Santiago, F.; Mora-Seró, I.; Garcia-Belmonte, G.; Giménez, S. Electron Lifetime in Dye-Sensitized Solar Cells: Theory and Interpretation of Measurements. *J. Phys. Chem. C* **2009**, *113*, 17278−17290.
(29) Mandujano-Ramirez, H. J.; Gonzalez-Vazquez, J. P.; Oskam, G.; Dittrich, T.; Garcia-Belmonte, G.; Mora-Sero, I.; Bisquert, J.; Anta, J. A. Charge Separation at Disordered Semiconductor Heterojunctions from Random Walk Numerical Simulations. *Phys. Chem. Chem. Phys.* **2014**, *16*, 4082−4091.
(30) Shi, J.; Xu, X.; Li, D.; Meng, Q. Interfaces in Perovskite Solar Cells. *Small* **2015**, *11*, 2472−2486.
(31) Frost, J. M.; Butler, K. T.; Walsh, A. Molecular Ferroelectric Contributions to Anomalous Hysteresis in Hybrid Perovskite Solar Cells. *APL Mater.* **2014**, *2*, 081506.
(32) Juarez-Perez, E. J.; Wuβler, M.; Fabregat-Santiago, F.; Lakus-Wollny, K.; Mankel, E.; Mayer, T.; Jaegermann, W.; Mora-Sero, I. Role of the Selective Contacts in the Performance of Lead Halide Perovskite Solar Cells. *J. Phys. Chem. Lett.* **2014**, *5*, 680−685.
(33) Peter, L. M. Characterization and Modeling of Dye-Sensitized Solar Cells. *J. Phys. Chem. C* **2007**, *111*, 6601−6612.
(34) van de Lagemaat, J.; Frank, A. J. Nonthermalized Electron Transport in Dye-Sensitized Nanocrystalline TiO2 Films: Transient Photocurrent and Random-Walk Modeling Studies. *J. Phys. Chem. B* **2001**, *105*, 11194−11205.
(35) Bisquert, J.; Vikhrenko, V. S. Interpretation of the Time Constants Measured by Kinetic Techniques in Nanostructured Semiconductor Electrodes and Dye-Sensitized Solar Cells. *J. Phys. Chem. B* **2004**, *108*, 2313−2322.
(36) Anta, J. A.; Mora-Seró, I.; Dittrich, T.; Bisquert, J. Interpretation of Diffusion Coefficients in Nanostructured Materials from Random Walk Numerical Simulation. *Phys. Chem. Chem. Phys.* **2008**, *10*, 4478−4485.
(37) Anta, J. A.; Idígoras, J.; Guillén, E.; Villanueva-Cab, J.; Mandujano-Ramírez, H. J.; Oskam, G.; Pellejà, L.; Palomares, E. A Continuity Equation for the Simulation of the Current−Voltage Curve and the Time-Dependent Properties of Dye-Sensitized Solar Cells. *Phys. Chem. Chem. Phys.* **2012**, *14*, 10285−10299.
(38) O'Regan, B. C.; Barnes, P. R. F.; Li, X.; Law, C.; Palomares, E.; Marin-Beloqui, J. M. Optoelectronic Studies of Methylammonium Lead Iodide Perovskite Solar Cells with Mesoporous TiO_2: Separation of Electronic and Chemical Charge Storage, Understanding Two Recombination Lifetimes, and the Evolution of Band Offsets During J−V Hysteresis. *J. Am. Chem. Soc.* **2015**, *137*, 5087−5099.
(39) Eames, C.; Frost, J. M.; Barnes, P. R. F.; O'Regan, B. C.; Walsh, A.; Islam, M. S. Ionic Transport in Hybrid Lead Iodide Perovskite Solar Cells. *Nat. Commun.* **2015**, *6*, 7497.
(40) Christians, J. A.; Manser, J. S.; Kamat, P. V. Best Practices in Perovskite Solar Cell Efficiency Measurements. Avoiding the Error of Making Bad Cells Look Good. *J. Phys. Chem. Lett.* **2015**, *6*, 852−857.

DOI: 10.1021/acs.jpclett.5b01696
J. Phys. Chem. Lett. 2015, 6, 3923−3930